The *Nkx2.3–Nr5a1* gene cascade plays a crucial role in spleen-specific vascular architecture and marginal zone formation

Kanako Miyabayashi[1*], Koji Ono[2*†], Tetsuya Sato[3], Ayano Yahagi[4§], Masanori Iseki[4], Katsuhiko Ishihara[4¶], Takami Mori[5‡], Miki Inoue[1], Ryuki Shimada[6], Kei-ichiro Ishiguro[7], Tomohiro Ishii[8], Jongsung Noh[9], Man Ho Choi[9], Takashi Baba[10], Yasuyuki Ohkawa[11], Emi Kiyokage[5], Kazunori Toida[2], Yuichi Shima[1]

[1]Division of Microscopic and Developmetal Anatomy, Department of Anatomy, Kurume University, School of Medicine, 67 Asahi-machi, Kurume, Fukuoka 830-0011, Japan

[2]Department of Anatomy, Kawasaki Medical School, 577 Matsushima, Kurashiki, Okayama 701-0192, Japan

[3]Biomedical Research Center, Faculty of Medicine, Saitama Medical University, 1397-1 Yamane, Hidaka, Saitama 350-1241, Japan

[4]Department of Immunology and Molecular Genetics, Kawasaki Medical School, 577 Matsushima, Kurashiki, Okayama 701-0192, Japan

[5]Department of Medical Technology, Kawasaki University of Medical Welfare, 288 Matsushima, Kurashiki, Okayama 701-0193, Japan

[6]Department of Chromosome Biology, Institute of Molecular Embryplogy and Genetics (IMEG), Kumamoto University, Kumamoto, Japan

[7]Department of Biomedical Science, Graduate School of Medicine, Chiba University, 260-8670, Japan

[8]Department ot Pediatrics, Keio University School of Medicine, Tokyo 160-8582, Japan

[9]Center for Advanced Biomolecular Recognition, Korea Institute of Science and Technology, Seoul, Korea

[10]Department of Molecular Biology, Graduate School of Medical Sciences, Kyushu University, Fukuoka, Japan

[11]Division of Transcriptomics, Medical Institute of Bioregulation, Kyushu University, Fukuoka, Japan

[*]These authors equally contributed to the work

[†]Present address: Faculty of Health and Medical Care, School of Medical Technology, Saitama Medical University, 1397-1 Yamane, Hidaka, Saitama 350-1241, Japan

[§]Present address: Department of Microscopic Anatomy and Developmental Biology, Tokyo Women's Medical University, 8-1, Kawada-cho, Tokyo 112-8681, Japan

[¶]Present address: Department of Design for Medical and Health Care, Faculty of Health and Welfare Services Administration, Kawasaki University of Medical Welfare, 288 Matsushima, Kurashiki, Okayama 701-0193, Japan

[‡]Present address: Department of Clinical Laboratory, Saga University Hospital, 5-1-1 Nabeshima, Saga 849-8501, Japan

Corresponding author: Yuichi Shima, M.D., Ph.D.
Division of Microscopic and Developmetal Anatomy, Department of Anatomy, Kurume University, School of Medicine, 67 Asahi-machi, Kurume-shi, Fukuoka 830-0011, Japan
Tel: +81 942 35 3311 (ext. 3150)
e-mail: yshima@kurume-u.ac.jp

Grants: This work was supported by JSPS (Japan Society for the Promotion of Science) KAKENHI Grant numbers 19K07378 (Y.S.), 23K19458, and 24K09992 (K.M.); Ryobi Teien Memory Foundation (Y.S.); Wesco Scientific Promotion Foundation (Y.S.); Research Project Grant from Kawasaki Medical School (R01B to K.O. and Y.S.); Startup Award for Researchers with Life Events at Kurume University (K.M.); and Grant from Kurume University for the Promotion of female researcher (K.M.).

Abstract

NR5A1 is a nuclear receptor and master regulator of steroidogenic tissue development and steroid hormone biosynthesis in the adrenal glands and gonads. While NR5A1 is expressed in splenic vascular endothelial cells, its functional role in the adult spleen remains poorly understood. Using single-cell transcriptomics in mice, here, we showed that NR5A1-positive endothelial cells were heterogeneous, with distinct phenotypes tied to their location in the splenic sinus versus the marginal sinus. To determine its function, we generated a spleen-specific *Nr5a1* enhancer deletion model. Loss of the enhancer led to reduced spleen size and ablation of both the marginal zone and marginal sinus. Moreover, 21α-hydroxylase activity in splenic sinusoidal endothelial cells was markedly diminished—especially in females—resulting in lower levels of adrenocortical steroids in the spleen. Enhancer deletion also induced ectopic lymphatic-like and high endothelial venule-like vasculature. These "lymph node–like" structures mirror those seen in *Nkx2.3*-deficient mice, and mutation of the NKX2.3-binding motif within the enhancer completely abolished NR5A1 expression in the spleen. These results together reveal that an *Nkx2.3→Nr5a1* regulatory axis is essential for the morphological and functional differentiation of spleen-specific vascular endothelial cells, with implications for splenic architecture necessary for blood filtration and marginal zone formation.

Key words:

NR5A1, enhancer, spleen, red pulp, white pulp, splenic sinus, marginal sinus, marginal zone, lymphocytes, erythrocytes, macrophage

Introduction

The spleen is a major secondary lymphoid organ that integrates blood filtration with immune surveillance. Structurally, it is composed of red and white pulp. Blood entering the spleen is directed either into the red pulp or into the marginal sinus located at the interface between the red and white pulp. In the red pulp, erythrocytes exiting the central arteries enter the open circulation and subsequently re-enter the lumen of splenic sinuses through interendothelial slits between elongated sinusoidal endothelial cells[1]. This unique vascular organization functions as a blood filter, in which aged or inflexible erythrocytes are retained and phagocytosed by macrophages[2]. Meanwhile, the marginal sinus and the surrounding marginal zone constitute a specialized vascular niche that regulates cellular trafficking into the white pulp[3]. Several immune cell populations, including SIGNR1 (CD209b)-positive macrophages, macrophage receptor with a collagenous structure (MARCO)-positive marginal zone macrophages[4,5], CD169 (SIGLEC-1/sialoadhesin)-positive marginal zone metallophilic macrophages[6,7], and marginal zone B cells[8], reside in the marginal zone and contribute to immune surveillance of blood-borne antigens[9-11].

NR5A1 (also known as Ad4BP or steroidogenic factor-1) is a nuclear receptor essential for the development and function of steroidogenic tissues, including the adrenal glands and gonads[12]. NR5A1 is also expressed in splenic sinusoidal endothelial cells, and mice lacking *Nr5a1* exhibit markedly reduced spleen size during fetal development[13]. However, interpretation of these findings has been limited by early postnatal lethality due to adrenal insufficiency[14], leaving the role of NR5A1 in the adult spleen unresolved. Recent single-cell transcriptomic studies have shown that genes involved in steroid hormone biosynthesis are selectively expressed in splenic endothelial cells[15]. Although NR5A1 directly regulates steroidogenic enzyme expression in the adrenal cortex[16], whether NR5A1 controls steroidogenic programs or other specialized functions in splenic endothelial cells remains unknown.

NKX2.3 is a homeobox transcription factor that plays a crucial role in the formation of splenic venous sinuses. *Nkx2.3* (*Nkx2-3*) knockout mice exhibit defects in the spleen and gut-associated lymphoid tissues[17]. In particular, the marginal zone is severely disrupted in *Nkx2.3*-deficient spleens[18,19], and lymphoid cysts filled with lymphocytes and high endothelial venules (HEVs)—structures normally restricted to lymph nodes—develop in knockout spleens[20,21].

In this study, we combine single-cell transcriptomics with genetic perturbation to define the role of NR5A1 in splenic vascular endothelial cells. We show that NR5A1-positive endothelial cells comprise transcriptionally distinct populations within the splenic and marginal

112 sinuses and identify a spleen-specific enhancer that governs *Nr5a1* expression in these
113 compartments. Functional disruption of this enhancer reveals that endothelial NR5A1 is
114 indispensable for establishing spleen-specific vascular identity, marginal sinus formation, and
115 marginal zone organization. Furthermore, we demonstrate that NKX2.3 directly regulates this
116 enhancer, thereby defining an *Nkx2.3–Nr5a1* transcriptional axis that plays a crucial role in
117 establishing vascular identity and functional architecture in the spleen.
118

Materials and Methods

Mouse strains

Ad4BP-BAC-EGFP mice[22] were used to visualize NR5A1-expressing sinus endothelial cells and to isolate NR5A1-positive cells. StAR/eGFP mice have been described previously[23]. ΔSpE mice were generated using genome editing[24-26]. Guide RNAs flanking the SpE were designed using CRISPR Direct (http://crispr.dbcls.jp/), and crRNA, tracrRNA, and Cas9 protein (Integrated DNA Technologies) were mixed and introduced into fertilized eggs by electroporation (Genome Editor, BEX). For SpE-R2m mice, a guide RNA targeting the R2 sequence and donor DNA carrying a mutated R2 sequence (R2m) were used. Edited embryos were transferred into recipient oviducts, and the genotypes were determined by PCR, with R2m integration confirmed by *Bam*HI digestion. Guide RNA and genotyping primer are provided in Supplemental Table 1. All animal experiments were approved by the Animal Care and Use Committee of Kawasaki Medical School and Kurume University School of Medicine.

Single-cell transcriptome analyses of NR5A1^{+} endothelial cells

Ad4BP-BAC-EGFP mice were sacrificed at approximately P70, and spleens were collected (n = 3; 2 males and 1 female). Spleens were minced, digested with collagenase (Nacalai Tesque), and EGFP-positive cells were isolated by fluorescence-activated cell sorting (FACS) using BD FACSAria III (BD) or CytoFLEX SRT (Agilent Biotechnologies). Sorted cells were processed for scRNA-seq using the 10x Genomics Chromium Single Cell 3′ Library & Gel Bead Kit v3.1, following the manufacturer's protocol, and libraries were sequenced on an Illumina NovaSeq 6000.

FASTQ files were processed with Cell Ranger (v9.0.0) using default settings and aligned to a custom reference genome generated by appending the EGFP cDNA sequence to mm10. Feature-barcode matrices were generated using the "count" pipeline. Subsequent analyses were performed in R using Seurat (v5.1.0)[27]. Cells with < 500 detected genes, > 6,000 UMIs, or > 10% mitochondrial reads were excluded. Doublets were removed using DoubletFinder (v2.0.6)[28], assuming a 7.5% of doublet rate and an optimal pK value determined by "find.pK". After quality filtering, including the EGFP expression, 31,199 cells were retained across three batches.

Gene expression data were normalized using "NormalizeData", and batch effects were corrected and integrated using Harmony[29]. Dimensionality reduction was performed by PCA, and the top 30 principal components were used for clustering with the Louvain algorithm

152 at a resolution of 0.1 using “FindClusters”. Clusters were visualized by UMAP using
153 “RunUMAP”. Differentially expressed genes (DEGs) were identified using “FindAllMarkers”
154 with the Wilcoxon rank-sum test and Bonferroni correction. Marker genes were defined as those
155 with an average log2 fold change ≥ 1 and an adjusted p-value < 0.01.
156 Functional annotation of cluster-specific markers was performed by Gene Ontology
157 (GO) enrichment analysis using clusterProfiler (v 4.17.0)[30]. For each cluster, the top 150 DEGs
158 ranked by log2 fold-change were analyzed using “compareCluster” and “enrichGO” with a q-
159 value cutoff of 0.01, across biological processes (BP), molecular functions (MF), and cellular
160 components (CC) categories.
161
162 ***Western blot analyses***
163 Nuclear extracts were prepared from adrenal glands and spleens (Nuclear Extraction Kit,
164 ab113474, Abcam) and quantified using a Qubit Protein Assay (Thermo Fisher Scientific).
165 Forty micrograms of protein was subjected to SDS-polyacrylamide gel electrophoresis and
166 western blot. Primary and secondary antibodies are listed in Supplemental Table 2.
167
168 ***Tissue preparation, histological studies, and immunostaining***
169 Mice were anesthetized with medetomidine hydrochloride (0.3 mg/kg; Nippon Zenyaku
170 Kogyo), midazolam (4 mg/kg; Astellas Pharma), and butorphanol tartrate (5 mg/kg; Meiji Seika
171 Pharma). Fresh tissues were collected, and bright-field or fluorescence images were acquired
172 using a stereomicroscope (Evident SZx10 or SZX16). For histology, mice were perfused with
173 PBS followed by 4% paraformaldehyde (PFA) in PBS, and tissues were further fixed by
174 immersion in 4% PFA.
175 Paraffin-embedded tissues were sectioned at 5 μm and stained with hematoxylin and
176 eosin (H&E). Images were acquired using a BZ-X700 (Keyence) and used to quantify white
177 pulp and total spleen areas with MZ-X Analyzer 1.3.0.3 (Keyence). For immunostaining, tissues
178 were sectioned at 50 μm using a CM3050 S cryotome (Leica) and stained by the free-floating
179 method[26]. Antibodies are listed in Supplemental Table 2. Nuclei were counterstained with DAPI
180 (Sigma), sections were mounted in VECTASHIELD (Vector Laboratories), and images were
181 acquired using a BZ-X700 (Keyence) or LSM 700 laser-scanning microscope (Zeiss).
182
183 ***Analyses of the circulating hemocytes***

184 Blood smear samples were stained with Giemsa, and erythrocytes containing Howell–Jolly
185 bodies was counted using a BX61 microscope equipped with a DP74 camera (Olympus). At
186 least 1,000 erythrocytes were analyzed per specimen (n = 4 per group).
187
188 ***Scanning electron microscopic (SEM) studies***
189 Spleens were fixed by interstitial perfusion[31] and immersion in 2.5% glutaraldehyde (TAAB)
190 and 4% PFA (Merck) in 0.1 M phosphate buffer (pH 7.4). Tissues were trimmed, post-fixed
191 with 1% OsO_4, incubated in 50% DMSO, freeze-fractured in liquid nitrogen, and post-fixed
192 again with 1% OsO_4. Specimens were treated with 2% tannic acid for 16 h and 2% OsO_4 for 6 h
193 using the tannin-osmium method[32], dehydrated through graded ethanol, transferred to *t*-butyl
194 alcohol, and freeze-dried. Fractured surfaces were mounted on metal stubs, coated with osmium
195 and platinum, and examined using an S-3400N scanning electron microscope (Hitachi) at 15
196 kV.
197
198 ***Bulk mRNA-sequencing, data processing, and differential gene expression analyses***
199 Bulk mRNA-seq was performed as previously described[25,26]. Total RNA from spleens or
200 endothelial cells sorted from Ad4BP-BAC-EGFP spleens was used for library preparation with
201 Illumina TruSeq (Illumina) or NEBNext Ultra RNA Library Prep Kit (New England Biolabs).
202 Libraries were sequenced on a NovaSeq 6000 with 150-bp paired-end reads. After adapter and
203 low-quality sequences removal using Cutadapt, reads were aligned to mm10 using STAR
204 (v2.7.3a). FeatureCounts (v2.0.1) and edgeR (v3.28.1) were used to calculate counts per million
205 (CPM). DEGs were identified using the criteria of $|\text{Log2FC}| \geq 2$, $p < 0.01$, and FDR < 0.01, and
206 were subjected to GO analyses using Metascape[33]
207 (https://metascape.org/gp/index.html#/main/step1).
208
209 ***Flow cytometry analyses***
210 Flow cytometry of splenic immune cells was performed as previously described[34]. Antibodies
211 used for the analyses are listed in Supplemental Table 2.
212
213 ***Measurement of steroid hormones in the spleen***
214 Spleens were collected from control and ΔSpE mice at approximately 10 weeks after birth (n =
215 3 per group). Steroid levels were determined by liquid chromatography-mass spectrometry (LC-
216 MS) following established methods[35,36] and are expressed as nanograms per gram of tissue. The

metabolic ratio for each enzymatic reaction was calculated by dividing the metabolite concentration by the precursor concentration.

Sequence data deposition in a public database

Sequencing data were deposited in the Gene Expression Omnibus (GEO): bulk spleen RNA-seq (GSE303957), bulk RNA-seq of sorted NR5A1-positive cells (GSE303956), and scRNA-seq of sorted NR5A1-positive cells (GSE303958).

Statistical analyses

At least three animals were used per group unless otherwise specified. Data are presented as the mean ± SEM. Two-group comparisons were performed using two-tailed Student's *t*-test, and multiple group comparisons by one-way ANOVA followed by Tukey–Kramer post hoc test; $p < 0.05$ was considered statistically significant.

231 **Results**

232 ***Spatial heterogeneity of NR5A1-expressing endothelial cells in the spleen***

233 NR5A1 is expressed in the splenic vascular endothelial cells[13], but its distribution in adult
234 spleens has not been thoroughly investigated. We therefore analyzed EGFP expression in
235 Ad4BP-BAC-EGFP mice[15], which faithfully recapitulate endogenous NR5A1 expression. EGFP
236 showed a macroscopically heterogeneous pattern, with strong signals in the red pulp (Fig. 1A,
237 A'). Immunostaining confirmed near-complete overlap between EGFP and endogenous NR5A1
238 (Fig. S1). Co-staining with CD3ε and CD45R indicated that EGFP was predominantly
239 expressed in endothelial cells of splenic sinusoids in the red pulp (Fig. 1B, C).

240 To further localize EGFP-positive cells, we compared EGFP expression with
241 macrophage markers (F4/80, MARCO, and CD169) and a marker for marginal sinus-lining cells
242 (mucosal vascular addressin cell adhesion molecule-1 [MAdCAM-1][37]). EGFP was detected
243 adjacent to F4/80-positive macrophages in the red pulp (Fig. 1D-D'') and in the marginal zone
244 containing MARCO-positive macrophages (Fig. 1E-E''). CD169-positive metallophilic
245 macrophages flanked the marginal sinus[7], consistent with EGFP expression in marginal sinus
246 endothelial cells (Fig. 1F-F''). MAdCAM-1 was detected in thin cells closely associated with
247 EGFP-positive cells (Fig. 1G-G'', Fig. S2). Together, these results demonstrate that NR5A1 is
248 expressed in endothelial cells of both the splenic and marginal sinuses. Figure 1H summarizes
249 the schematic representation of spatial distribution of NR5A1-positive cells and other cell types
250 in the marginal sinus and marginal zone.

251

252 ***Functional differences between endothelial cells of the splenic sinus and marginal sinus***

253 We performed scRNA-seq on EGFP-positive cells isolated from Ad4BP-BAC-EGFP spleens.
254 Dimensional reduction and clustering of cells from three mice (two males and one female)
255 yielded highly similar patterns across samples (Fig. S3A) and identified six clusters, including
256 two major populations (clusters 1 and 2; Fig. 2A). *Egfp*, *Nr5a1*, and the sinusoidal endothelial
257 marker *Stab2* were broadly detected, confirming dataset validity (Fig. S3B-D).

258 To assign anatomical identities, we focused on *Star* and *Cd34*, enriched in clusters 1
259 and 2, respectively (Fig. 2B, C). Immunostaining of Ad4BP-BAC-EGFP spleens showed
260 marginal sinus-selective localization of CD34 (Fig. 2D). Meanwhile, Immunostaining of
261 StAR/eGFP spleens revealed that StAR-positive cells were largely CD34-negative (Fig. 2E),
262 localized outside the marginal zone (Fig. 2F), and enriched in the red pulp near F4/80-positive

263 macrophages (Fig. 2G). Thus, clusters 1 and 2 correspond to splenic sinus and marginal sinus
264 endothelial cells, respectively.
265 Although canonical endothelial markers (*Pecam1*, *Cdh5*, *Eng*, and *Erg*) were
266 detected in all clusters (Fig. S3E), GO analysis of the DEGs revealed distinct transcriptional
267 programs in each cluster (Fig. 2H, Fig. S4; Supplemental Table 3). Cluster 1 was enriched for
268 genes associated with negative chemotaxis and vascular guidance (*Flrt2*, *Sema3d*, *Robo2*, *Itga9*,
269 *Mmp28*) and extracellular matrix organization (*Adamts5*, *Col23a1*) (Fig. 2H, I, Fig. S3F). In
270 addition, several genes enriched in cluster 1 encode guidance molecules or regulators of
271 endothelial fate, including *Jag1* and *Gli3*, and factors involved in matrix remodeling and
272 vasculogenic patterning[38]. In contrast, cluster 2 showed enrichment for genes linked to
273 endothelial migration and angiogenesis (*Ptp4a3*, *Dll4*, *Col18a1*, *Kdr*, *Id1*, *Adamts9*, *Amotl2*,
274 *Esm1*, *Mcam*, *Emcn*) (Fig. 2H, J, Fig. S3G), including markers of endothelial tip cell markers;
275 *Esm1*, *Dll4*, *Kdr*, and *Id1*[39-42], and genes mediating cell–cell and cell–matrix interactions; *Esam*,
276 *Col18a1*, *Adamts9*, and *Mcam*[43] (Fig. 2J, Fig. S3G), indicating active angiogenic remodeling in
277 marginal sinus.
278 Among the minor clusters, cluster 3 was enriched for ribosomal genes, suggesting
279 low-quality cells; cluster 4 exhibited intermediate profile between clusters 1 and 2; Cluster 5
280 was enriched for mitotic genes, consistent with proliferating cells; and cluster 6 expressed
281 markers of neutrophils and lymphocytes (*Ikzf1*, *Igkc*, *Ly6d*), consistent with doublets or
282 contamination (Fig. 2H, Fig. S3H, Fig. S4).
283
284 ***Identification of the SpE in the Nr5a1 gene***
285 We previously identified multiple tissue-specific enhancers within the *Nr5a1* locus[44-47] (Fig.
286 3A), and demonstrated the functional importance of each enhancer by deleting it from the
287 mouse genome[25,26]. Given the high degree of conservation in enhancer regions, we focused on a
288 conserved sequence within the fourth intron and generated mice with 441-bp deletion by
289 CRISPR/Cas9 (Fig. 3A, B, Fig. S5), resulting in complete loss of NR5A1 expression in the
290 spleen (Fig. 3C). We designated this region the spleen enhancer (SpE) and homozygous mutants
291 as ΔSpE mice.
292 Heterozygous deletion had no gross effect on spleen size, whereas ΔSpE mice
293 exhibited marked size reductions (Fig. 3D). Because spleens exhibit sex differences in size and
294 weight[48], analyses were conducted in both sexes. These analyses revealed a significant reduction

295 in spleen weight in ΔSpE mice compared with wild type (WT) (Fig. 3E). In contrast, adrenal
296 glands and gonads were unaffected (Fig. S6), indicating spleen-specific activity of SpE.
297
298 ***Structural and functional abnormality in ΔSpE spleens***
299 H&E staining showed island-like white pulp embedded in red pulp in WT spleens, whereas
300 ΔSpE exhibited centrally fused white pulp surrounded by a thin layer of red pulp (Fig. 4A). The
301 white pulp-to-red pulp ratio increased only in female ΔSpE mice (Fig. 4B). WT spleens
302 displayed a well-defined marginal zone and marginal sinus (Fig. 4C), whereas both structures
303 were absent in ΔSpE mice (Fig. 4D).
304 Immunostaining revealed that, in ΔSpE spleens, segregation of B and T cells was
305 largely preserved; however, neither the marginal zone nor the laminin-positive marginal sinuses
306 were detectable (Fig. 4E, F). Notably, MARCO- and CD169-positive macrophages were
307 partially disrupted in heterozygote and absent in ΔSpE spleens (Fig. 4G–I). In addition, flow
308 cytometry analyses revealed reduced $CD21^{hi}/CD23^{low/-}$ marginal zone B cells[8] and transitional B
309 cells of type 1 (T1B), whereas other immune cell populations were unaffected (Fig. S7).
310 Together, these findings demonstrate that SpE-mediated *Nr5a1* expression is
311 required for formation of the marginal sinus and marginal zone.
312
313 ***Decreased steroidogenic activity in ΔSpE spleen***
314 Bulk RNA-seq of WT and ΔSpE spleens as well as EGFP-positive cells (splenic endothelial
315 cells; SECs) isolated by FACS from Ad4BP-BAC-EGFP mice was performed to
316 comprehensively explore the functional changes in ΔSpE spleens. Comparison of WT and ΔSpE
317 spleens revealed a greater number of downregulated genes in females than in males (1,059 vs.
318 552 genes), prompting sex-stratified analyses. Among SEC-enriched genes downregulated in
319 ΔSpE spleens (159 in males and 132 in females), 88 genes were shared between the sexes (Fig.
320 5A, B; Supplemental Table 4). These shared genes were enriched for GO terms associated with
321 adrenal hormone biosynthesis pathways (Fig. S8), including *Star* and *Cyp21a1* (Fig. 5C-E).
322 We focused on CYP21A1, an enzyme essential for adrenocortical steroid hormone
323 production and confirmed that *Cyp21a1* expression was nearly abolished in ΔSpE spleens (Fig.
324 5E). LC-MS demonstrated reduced conversion of progesterone to 11-deoxycorticosterone in
325 ΔSpE spleens, with a strong effect in females (Fig. 5F; Fig. S9A). Single-cell data confirmed
326 expression of *Star* and *Cyp21a1* in splenic sinus endothelial cells, whereas other steroidogenic
327 enzymes were minimally or not expressed (Fig. 5G, Fig. S9B). Collectively, these findings

328 indicate that splenic sinus endothelial cells possess partial steroidogenic capacity, and that this
329 capacity is dependent on NR5A1.
330
331 ***Lymph node-like structures and fibrosis in ΔSpE spleens***
332 Genes upregulated in ΔSpE spleens were compared between males and females (798 in males
333 and 726 in females) (Fig. 6A, 6B) and GO analyses of the genes shared between sexes (427
334 genes in Supplemental Table 5) revealed enrichment for cell migration and lumen formation
335 (Fig. S10). Notably, the gene set included the lymphatic marker *Lyve1* and HEV-associated
336 genes *Glycam1* and *Emcn* (Fig. 6C, D). Immunostaining revealed that LYVE-1- and MECA79-
337 positive structures were almost absent in WT spleens, partially developed in heterozygotes, and
338 clearly detectable in ΔSpE spleens, as well as in mesenteric lymph nodes (Fig. 6E–H).
339 MAdCAM-1 was expressed in marginal sinus-lining cells in WT spleens but was weakly
340 detectable in the red pulp of heterozygotes. In ΔSpE spleens, MAdCAM-1-positive vessels were
341 well developed in the red pulp and closely resembled HEVs in mesenteric lymph nodes (Fig.
342 6I–L).
343 Scanning electron microscopy revealed replacement of fenestrated sinusoids by tall
344 HEV-like vessels (Fig. 6M, N), accompanied by an increased number of abnormal erythrocytes,
345 including Howell–Jolly bodies, in the peripheral blood (Fig. S11). Upregulated genes in ΔSpE
346 spleens were also enriched for extracellular matrix organization and elastic fiber formation (Fig.
347 S10), and immunostaining confirmed increased laminin-encased vessels and reduced red pulp
348 macrophages (Fig. S12).
349
350 ***NKX2.3 regulates Nr5a1 expression via direct binding to the SpE***
351 Within the SpE, we identified several small subregions with sequences conserved across
352 mammalian species (Fig. S5B). One of these subregions, designated R2, contained a predicted
353 NKX2.3-binding motif (Fig. 7A). Mutation of this site (SpE-R2m; Fig. 7B) resulted in reduced
354 spleen size, complete loss of NR5A1 expression, absence of the marginal sinus and marginal
355 zone, and the development of ectopic lymphatic- and HEV-like structures (Fig. 7C–K), closely
356 resembling the phenotypes of ΔSpE mice.
357 *Nkx2.3* knockout mice exhibit similar phenotypes[20,21,49], and our scRNA-seq data
358 showed *Nkx2.3* is expressed in splenic and marginal sinus endothelial cells, independent of
359 NR5A1 deletion (Fig. S13). Together, these results demonstrate that NKX2.3 directly regulates
360 *Nr5a1* expression through the SpE in splenic endothelial cells.

361

Discussion

NR5A1 defines functionally distinct endothelial populations in the splenic sinus and marginal sinus

The spleen performs two tightly coupled vascular functions: filtration of circulating blood and initiation of immune responses. These functions are spatially segregated and associated with the splenic[1] and marginal sinuses[3,8,9,11,50,51], respectively. Our single-cell transcriptomic analyses resolved NR5A1-positive endothelial cells into two clusters corresponding to their anatomical localization. Marginal sinus endothelial cells were enriched for genes involved in vascular patterning and ECM remodeling, whereas splenic sinus endothelial cells preferentially expressed genes linked to angiogenesis and cell–substrate adhesion. Notably, marginal sinus endothelial cells expressed higher levels of *Cd34*, a marker of immature or progenitor-like endothelial states[52], suggesting that they are less differentiated than splenic sinus endothelial cells. Together, these data indicate that NR5A1 marks heterogeneous endothelial populations with compartment-specific transcriptional programs. Defining their developmental relationship will be an important subject of future studies.

NR5A1-dependent gene programs shape splenic vascular architecture and steroidogenic capacity

Deletion of the SpE caused marked disruption of splenic architecture, including loss of the marginal sinus and marginal zone, indicating that NR5A1 is required for morphological differentiation of spleen-specific vasculature. In addition, ΔSpE spleens showed reduced expression of *Star* and *Cyp21a1*, key enzymes in adrenal steroidogenesis. Given NR5A1's established role in regulating these genes in adrenocortical cells, it is likely that NR5A1 similarly controls their expression in splenic sinus endothelial cells.

Although additional enzymes required for complete adrenal steroidogenesis were not detected in NR5A1-positive splenic cells, adrenal-type steroids were present in whole-spleen extracts, suggesting cooperation between NR5A1-positive endothelial cells and other splenic cell types. To our knowledge, this represents the first evidence of adrenal-type steroid hormone production in the spleen, although its physiological significance remains unclear.

The severe vascular disorganization in ΔSpE mice further indicates that NR5A1 regulates downstream gene networks beyond steroidogenesis. Single-cell analyses suggest that *Star* and *Cyp21a1* are selectively regulated by NR5A1 in splenic sinus endothelial cells, whereas NR5A1 targets in marginal sinus endothelial cells remain undefined. Because the

395 marginal zone provides a microenvironment for macrophages and B cells essential for immune
396 surveillance of blood-borne antigens, defective marginal sinus formation likely disrupts immune
397 organization. Thus, NR5A1 coordinates both the structural and functional specialization of
398 spleen-specific vasculature.

399 Sex-specific differences were also evident. Loss of NR5A1 activity produced more
400 pronounced phenotypes in females, including a greater reduction in CYP21A1 expression and
401 altered white pulp–to–red pulp ratios. These findings suggest that NR5A1-dependent vascular
402 and steroidogenic programs are modulated in a sex-dependent manner, potentially reflecting
403 differences in baseline expression, developmental timing, or interactions with sex hormone
404 signaling. Sex differences in immune function are well established in mice and humans[53], and
405 because circulating adrenal steroid hormone levels also show sexual dimorphism, spleen-
406 derived adrenal-type steroid production may contribute to these differences and possibly to
407 immune-related pathologies.
408

409 **An Nkx2.3–Nr5a1 enhancer axis quantitatively controls spleen-specific vascular**
410 **development**

411 Although the spleen shares features with other secondary lymphoid organs, NR5A1 expression
412 was restricted to the spleen and absent from lymph nodes and gut-associated lymphoid tissue.
413 We further demonstrate that NKX2.3 binding to the SpE is indispensable for splenic NR5A1
414 expression, thereby establishing an *Nkx2.3→Nr5a1* regulatory axis that underlies spleen-
415 specific endothelial differentiation.

416 The mechanism conferring spleen specificity to the SpE remains unresolved.
417 Sequences outside the NKX2.3-binding region may contribute to this specificity, and additional
418 regulatory elements within the *Nr5a1* locus, including potential shadow enhancers, may
419 modulate expression robustness. Moreover, previous work implicating Polycomb group proteins
420 in *Nr5a1* regulation[54] suggests that chromatin-based mechanisms cooperate with the SpE to
421 fine-tune NR5A1 expression.

422 Our analysis further demonstrates that *Nr5a1* expression is dosage sensitive.
423 Heterozygous SpE deletion or mutation resulted in a much milder phenotype than homozygous
424 deletion, indicating that NR5A1 levels quantitatively regulate spleen development. This dose
425 dependence is consistent with previous reports linking NR5A1 dosage to cell differentiation and
426 tissue morphogenesis[55] and likely reflects enhancer redundancy, whereby loss of a single
427 enhancer produces a weaker phenotype than homozygous deletion[56]. Clinically, NR5A1

428 haploinsufficiency causes variable adrenal and gonadal phenotypes in humans[57,58]. Our findings
429 extend this concept to the spleen, showing that even modest reductions in NR5A1 perturb
430 vascular organization and reinforcing the principle that transcription factor dosage quantitatively
431 shapes organ development.
432

Acknowledgements

We appreciate the technical support provided by the Central Research Center, Kawasaki Medical School, and the Institute for Disease Modeling, Kurume University School of Medicine. We also thank the organizers of the Medical Research Center at Saitama Medical University for providing continuous support throughout this study. This study was supported by the Research Program for the Inter-University Research Network for High-Depth Omics, IMEG, Kumamoto University, Japan. This work was supported in part by the MEXT Promotion of Development of a Joint Usage/Research System Project: Pan-Omics DDRIC, MRCI for High-Depth Omics, CURE: JPMXP1323015486 for MIB, RIIT, and the Autonomous Medical Research Center at Kyushu University. We would like to thank Editage (www.editage.jp) for English language editing.

Author contributions

Conceptualization, Y. S.; Investigation, K. M., K. O., Miki Inoue, T. S., A. Y., Masanori Iseki, Katsuhiko Ishihara, T. M., R. S., Kei-ichirou Ishiguro, J. N., M. H. C., T. B., Y. O., E. K., K. T., and Y. S.; Resources, T. I.; Format analysis and Writing – Original Draft Preparation, K. M., K.O., and Y. S.; Writing – Review & Editing, T. S., A. Y., Masanori Iseki, Katsuhiko Ishihara, T. M., Miki Inoue, R. S., Kei-ichirou Ishiguro, M. H. C., T. B., Y. O., E. K., K. T., and Y. S.; Funding Acquisition, K. M., K. O., Y. S., and Supervision, Y. S.

Competing interests

The authors have no conflicts of interest to disclose.

456 ***Figure Legends***

457 Figure 1. **EGFP expression in the spleen of Ad4BP-BAC-EGFP mice.**

458 (A, A') Macroscopic view of WT and Ad4BP-BAC-EGFP mouse spleens under bright-field (A)
459 and EGFP fluorescence (A') microscopy. The WT spleen is outlined with a white dotted line in
460 A'. Bar = 500 μm.

461 (B, C) Immunostaining for EGFP together with CD3ε and CD45R in Ad4BP-BAC-EGFP
462 mouse spleens, shown with (B) or without (C) DAPI nuclear counterstaining. Bar = 100 μm.

463 (D-D'', E-E'', F-F'', G-G'') Immunostaining of EGFP with cell type-specific markers: F4/80
464 (D-D''), MARCO (E-E''), CD169 (F-F''), and MAdCAM-1 (G-G''). Arrows indicate EGFP
465 expression in the endothelial cells of the venous sinuses in the red pulp (splenic sinuses), and
466 arrowheads indicate EGFP expression in the endothelial cells of the venous sinuses at the border
467 between the white pulp and the marginal zone (marginal sinuses). Bar = 50 μm.

468 (H) Schematic illustration of the histological structure of the marginal zone and marginal sinus,
469 showing the cell types observed in this region. RP, red pulp; WP, white pulp.

470

471 Figure 2. **Functional and spatial heterogeneity of EGFP-positive endothelial cells in the**
472 **spleens of Ad4BP-BAC-EGFP mice.**

473 (A) UMAP plot of clusters consisting of EGFP-positive endothelial cells isolated from Ad4BP-
474 BAC-EGFP spleens.

475 (B–C) Feature plots of representative genes expressed in EGFP-positive endothelial cells: *Star*
476 (B) and *Cd34* (C).

477 (D) Immunostaining of EGFP and CD34 in Ad4BP-BAC-EGFP spleens. Arrows indicate
478 CD34/EGFP double-positive cells.

479 (E-G) Immunostaining of EGFP with CD34 (H), MARCO (I), or F4/80 (J) in StAR/eGFP
480 spleens. Arrows in (E) indicate small number of CD34/EGFP double-positive cells in
481 StAR/eGFP spleens. Bar = 100 μm. RP, red pulp; WP, white pulp.

482 (H) Bubble plot showing the biological processes characterizing each cluster. The top 150
483 highly expressed genes in each cluster were used for GO analysis.

484 (I) Feature plots of representative genes highly expressed in cluster 1: *Flrt2*, *Sema3d*, *Adamts5*,
485 *Ccbe1*, *Itga9*, and *Jag1*.

486 (J) Feature plots of representative genes highly expressed in cluster 2: *Ptp4a3*, *Dll4*, *Kdr*,
487 *Adamts9*, *Esm1*, and *Esam*.

488

489 Figure 3. **Spleen-specific depletion of NR5A1 by deletion of the spleen enhancer (SpE) of**
490 **the *Nr5a1* gene.**
491 (A) Schematic representation of the *Nr5a1* gene structure and sequence conservation among
492 mammals. Gray boxes indicate previously identified enhancers, including fetal Leydig enhancer
493 (FLE), fetal adrenal enhancer (FAdE), ventromedial hypothalamus enhancer (VE), and pituitary
494 enhancer (PE). The yellow box indicates the spleen enhancer (SpE) located in intron 4. Arrows
495 (SpE-Fw and SpE-Re) denote genotyping primers.
496 (B) PCR-based genotyping of SpE-deleted mice. The WT allele yields a 655-bp fragment,
497 whereas the SpE-deleted allele yields a 213-bp fragment.
498 (C) Loss of NR5A1 expression in the spleens of ΔSpE mice. Western blot analysis of NR5A1
499 and LaminB1 in nuclear extracts from spleens of WT (+/+), heterozygous (+/-), and
500 homozygous (-/-) SpE-deleted mice.
501 (D) Gross morphology of spleens from WT, heterozygote (Het), and ΔSpE mice.
502 (E) Spleen weight-to-body weight ratio in each genotype and sex (mean ± SE). Sample size:
503 male WT, n = 12; male ΔSpE, n = 6; female WT n = 9; female ΔSpE, n = 5. $p < 0.01$ (**).
504
505 Figure 4. **Morphological analysis of ΔSpE spleens.**
506 (A) Hematoxylin and eosin (H&E) staining of spleens from each genotype and sex. Scale bar =
507 2 mm
508 (B) White pulp-to-red pulp area ratios in each genotype and sex. Sample sizes: male WT, n = 6;
509 male ΔSpE, n = 4; female WT n = 5; female ΔSpE, n = 3. $p < 0.01$ (**).
510 (C, D) High-magnification H&E-stained images of WT and ΔSpE spleens. Arrows indicate
511 marginal sinuses. Scale bar = 100 μm.
512 (E, F) Immunostaining of CD45R, CD3ε, and laminin in WT and ΔSpE spleens. RP, red pulp;
513 WP, white pulp; MZ, marginal zone. Scale bar = 100 μm.
514 (G., H., I) Immunostaining for MARCO and CD169 in WT, heterozygote (Het), and ΔSpE
515 spleens. Scale bar = 100 μm.
516
517 Figure 5. **Downregulated genes in ΔSpE spleens.**
518 (A) Schematic representation of the strategy for gene expression analyses. Comparison of gene
519 expression between WT spleens and sorted NR5A1^{+} sinusoidal endothelial cells (SECs)
520 identified genes enriched in SECs (Up in SEC). Comparison between WT and ΔSpE spleens

521 identified genes downregulated in ΔSpE (Down in ΔSpE). Genes included in both categories
522 (Up in SEC and Down in ΔSpE) were extracted for each sex.
523 (B) Venn diagram showing overlapping (Up in SEC and Down in ΔSpE) genes in both sexes.
524 (C) Schematic representation of steroid biosynthetic pathways, including steroidogenic
525 enzymes, precursors, and metabolites. Enzymes indicated in blue are among 88 genes identified
526 in (B). Metabolites indicated in red represent corticosteroid hormones and their precursors.
527 (D) Volcano plot of gene expression in WT and ΔSpE spleens. Genes in red indicate
528 representative genes downregulated in ΔSpE.
529 (E) Expression levels of *Cyp21a1* gene in WT and ΔSpE spleens in each sex, showing as counts
530 per million (CPM). $p < 0.01$ (**).
531 (F) Metabolic activity of 21α-hydroxylase, assessed by precursor and metabolite concentrations
532 in WT and ΔSpE spleens of each sex, determined by liquid chromatography-mass spectrometry
533 (LC-MS). $p < 0.05$ (*).
534 (G) Feature plot of *Cyp21a1* expression in a UMAP presentation of $NR5A1^+$ endothelial cells in
535 the spleen.
536
537 Figure 6. **Upregulated genes in ΔSpE spleens.**
538 (A) Schematic representation of the strategy for gene expression analyses. Comparison of gene
539 expression between WT and ΔSpE spleens identified genes upregulated in ΔSpE (Up in ΔSpE).
540 (B) Venn diagram showing (Up in ΔSpE) genes in both sexes.
541 (C) Volcano plot of gene expression in WT and ΔSpE spleens. Genes in red indicate
542 representative genes upregulated in ΔSpE.
543 (D) Expression levels of *Lyve1*, *Glycam1*, *and Emcn* genes in WT and ΔSpE spleens in each
544 sex, showing as counts per million (CPM). $p < 0.01$ (**).
545 (E, F, G, H) Immunostaining of LYVE-1 and MECA79 in WT, heterozygote (Het), ΔSpE
546 spleens and WT mesenteric lymph node (WT mLN). Scale bar = 100 μm.
547 (I, J, K, L) Immunostaining of LYVE-1 and MAdCAM-1 in WT, heterozygote (Het), ΔSpE
548 spleens and WT mesenteric lymph node (WT mLN). Scale bar = 100 μm.
549 (M, N) Scanning electron microscopy (SEM) images of WT and ΔSpE spleens. Scale bar = 50
550 μm.
551
552 Figure 7. **NKX2.3 regulates *Nr5a1* gene expression in the spleen via direct binding to SpE.**

553 (A) Schematic representation of a mutation induced in R2 sequence in SpE. The yellow box
554 indicates SpE, and arrows indicate genotyping primers (SpE-Fw and SpE-Re). The red open
555 rectangle indicates the R2 sequence, and asterisks indicate the NKX2.3-binding motif. Mutated
556 R2 sequence (R2m) contains *Bam*HI restriction element (*Bam*HI-RE). The consensus sequence
557 for human NKX2-3 binding was searched in JASPAR (https://jaspar.genereg.net/) and is shown
558 in PWM format.
559 (B) PCR-based genotyping of SpE-R2m mice. The WT allele yielded a 655-bp fragment,
560 whereas the SpE-R2m allele yielded 429-bp and 225-bp fragments.
561 (C) Gross morphology of spleens from WT (+/+) and homozygous mutation in SpE (SpE-R2m)
562 mice. Scale bar = 2 mm.
563 (D, E) Immunostaining of NR5A1 in WT and SpE-R2m spleens. Scale bar = 50 μm.
564 (F, G, H) Immunostaining of CD34 and MARCO in WT, heterozygote (Het) and SpE-R2m
565 spleens. Scale bar = 100 μm.
566 (I, J, K) Immunostaining of CD34 and MARCO in WT, heterozygote (Het), and SpE-R2m
567 spleens. Scale bar = 100 μm.
568

569 Supplemental Figure 1. **Comparison of endogenous NR5A1 and EGFP expression in the**
570 **spleens of Ad4BP-BAC-EGFP mice.**
571 Double immunostaining for NR5A1 (red) and EGFP (green) and nuclear counterstaining with
572 DAPI (blue) were performed on spleen sections from Ad4BP-BAC-EGFP mice. Images of the
573 same field are as follows: (A) NR5A1 channel; (B) EGFP channel; (C) merged NR5A1 and
574 EGFP; and (D) merged NR5A1, EGFP, and DAPI. Magnified views of the regions including the
575 marginal sinus are presented as A', B', C', and D', with arrowheads indicating endothelial cells
576 of the marginal sinus. Likewise, enlarged views of regions including the splenic sinus are shown
577 as A'', B'', C'', and D'', with arrows indicating the endothelial cells of the splenic sinus. Scale
578 bar = 50 μm.
579
580 Supplemental Figure 2 **Spatial relationship between EGFP-positive cells and MAdCAM-1-**
581 **positive cells in the spleen of Ad4BP-BAC-EGFP mice.**
582 (A) Immunofluorescence image of MAdCAM-1, EGFP, and Laminin, together with DAPI
583 nuclear staining, in the spleens of Ad4BP-BAC-EGFP mice. The region outlined by the yellow
584 box is shown enlarged in panel B. Scale bar = 50 μm The image in panel B is further separated
585 into individual channels: MAdCAM-1 (red) in panel C; laminin (white) in panel D; merged
586 MAdCAM-1 and EGFP in panel E; EGFP (green) in panel F; and DAPI (blue) in panel G.
587 Dotted lines in panels C, D, F, and G indicate MAdCAM-1-positive cells. (H) Line plot
588 generated along the direction indicated by the arrow in Panel B. The plot shows that EGFP-
589 positive cells (green) are adjacent to MAdCAM-1-positive cells (red). Scale bar = 10 μm
590
591 Supplemental Figure 3. **Gene expression profiles in each cluster of NR5A1+ cells in the**
592 **spleens of Ad4BP-BAC-EGFP mice.**
593 (A) UMAP plot of cells from three mice (two males and one female) after merging the datasets,
594 with cells colored according to their individual origin.
595 (B–D) Feature plots of representative genes expressed in EGFP-positive endothelial cells: *Egfp*
596 (B), *Nr5a1* (C), *Stab2* (D).
597 (E) Feature plots of representative genes commonly expressed in clusters 1 and 2.
598 (F) Feature plots of representative genes that were highly expressed in cluster 1.
599 (G) Feature plots of representative genes highly expressed in cluster 2.
600 (H) Feature plots of representative genes highly expressed in cluster 6 (highlighted with red
601 circles).

602

603 Supplemental Figure 4. **GO analysis of genes enriched in each cluster of NR5A1^{+} sinus**
604 **endothelial cells in the spleens of Ad4BP-BAC-EGFP mice.**
605 (A) Bubble plot showing the molecular functions associated with each cluster identified by
606 scRNA-seq in EGFP^{+} sinus endothelial cells. (B) Bubble plot showing the cellular components
607 associated with each cluster identified by scRNA-seq of EGFP^{+} sinus endothelial cells. Gene
608 Ontology (GO) analysis was performed using the top 150 highly expressed genes in each
609 cluster.
610

611 Supplemental Figure 5. **Schematic illustration of the SpE deletion by CRISPR/Cas9.**
612 (A) Two guide RNAs were designed to target the upstream and downstream regions of the SpE.
613 Arrows (SpE-Fw and SpE-Re) indicate the positions of the genotyping PCR primers. Nucleotide
614 sequences surrounding the guide RNA target sites are shown (WT, wild type; del, SpE
615 deletion). Guide RNA target sequences are shown in red, and PAM sequences are underlined.
616 (B) Alignment of the nucleotide sequences of SpE regions in mice, rats, rabbits, pigs, and dogs
617 using MAFFT (https://mafft.cbrc.jp/alignment/software/). Asterisks indicate nucleotides
618 conserved among all species. Guide RNA target sequences are shown in red, and PAM
619 sequences are underlined. Nucleotides boxed in red indicate the R2 sequence, the mutation of
620 which abolished enhancer activity.
621

622 Supplemental Figure 6. **Morphology of NR5A1-expressing organs other than the spleen in**
623 **ΔSpE mice.**
624 (A) Gross morphology of the adrenal glands in WT and ΔSpE mice.
625 (B) Gross morphology of the ovaries in WT and ΔSpE mice.
626 (C) Gross morphology of the testes in WT and ΔSpE mice.
627 Scale bar = 2 mm.
628

629 Supplemental Figure 7. **Flow cytometry analysis of splenic immune cells in ΔSpE mice.**
630 (A) Representative flow cytometry plot of the spleen. B: B cells (CD19^{+}), MZB: marginal zone
631 B cells (CD19^{+}CD21/35^{high}CD23$^{low/-}$), FoB: follicular B cells (CD19^{+}CD21/35^{high}CD23^{high}),
632 T1B: Transitional B cells of type1 (CD19^{+}CD21/35^{-}CD23^{-}), T2B: transitional B cells of type 2
633 (CD19^{+}CD23^{+}CD21/35^{+}IgM^{+}).

634 (B) Flow cytometry of B-cell subsets isolated from the spleen of a WT mouse.
635 CD21/35^{high}CD23$^{low/-}$ (marginal zone B cells) cells constitute 6.91% of CD19^{+} B cells.
636 (C) Flow cytometry of B-cell subsets isolated from the spleen of an SpE heterozygous mouse.
637 CD21/35^{high}CD23$^{low/-}$ cells constitute 7.38% of CD19^{+}B cells.
638 (D) Flow cytometry analysis of B-cell subsets isolated from the spleen of a ΔSpE mouse.
639 CD21/35^{high}CD23$^{low/-}$ cells constituted 0.66% of CD19^{+}B cells.
640 (E) Frequencies of B-cell subsets in the spleen: B: B cells, FoB: follicular B cells, T1B:
641 transitional B cells of type 1, T2B: transitional B cells of type 2, MZB: marginal zone B cells,
642 WT: wild-type: Het, heterozygous deletion of SpE, ΔSpE: deletion of SpE,*: $p < 0.05$, ns: not
643 significant.
644
645 Supplemental Figure 8. **GO analysis of genes downregulated in the spleens of ΔSpE mice.**
646 (A) Biological processes associated with the downregulated genes in ΔSpE spleens.
647 (B) Tissue specificity of genes downregulated in ΔSpE spleens.
648 (C) Transcription factors predicted to regulate the genes downregulated in ΔSpE spleens.
649
650 Supplemental Figure 9. **Steroid levels and expression of steroidogenic genes in the spleen.**
651 (A) The concentrations of progesterone and 11-deoxycorticosterone were measured by LC-MS.
652 M, male; F, female; WT, wild type.
653 (B) Feature plots showing the expression of the genes required for adrenal steroid production.
654 *Star* and *Cyp21a1* were expressed in cluster 1, whereas the expression of the other genes was
655 very low or undetectable (ND).
656
657 Supplemental Figure 10. **Upregulated genes in the spleens of ΔSpE mice.**
658 Biological processes identified by GO analysis of genes upregulated in the spleen of ΔSpE
659 mice.
660
661 Supplemental Figure 11. **Abnormal peripheral erythrocytes in ΔSpE mice.**
662 (A) Giemsa-stained peripheral blood samples from control male mouse.
663 (B) Giemsa-stained peripheral blood samples from a male ΔSpE mice. Arrows indicate
664 abnormal erythrocytes containing Howell–Jolly bodies. Scale bar = 20 μm.
665 (C) The proportion of erythrocytes containing Howell–Jolly bodies in control and ΔSpE mice of
666 each sex. At least 1,000 erythrocytes were examined per specimen (n = 4). $p < 0.01$ (**).

667

668 Supplemental Figure 12. **Increased ECM expression in the spleens of ΔSpE mice.**
669 (A–C) Double immunostaining for F4/80 (red) and Laminin (green) with nuclear
670 counterstaining using DAPI (blue) in the spleen sections. WT, wild type; Het, SpE
671 heterozygous. Scale bar = 100 μm.

672

673 Supplemental Figure 13. ***Nkx2-3* expression in the spleens of ΔSpE mice.**
674 (A) Feature plot showing *Nkx2-3* expression in NR5A1^{+} cells isolated from the spleens of
675 Ad4BP-BAC-EGFP mice. *Nkx2-3* is expressed in clusters 1 and 2.
676 (B) *Nkx2-3* expression in the spleens of WT and ΔSpE mice of both sexes, as revealed by
677 mRNA-sequence analysis. Expression levels are expressed as counts per million (CPM).

678

679 ***References***

680

681 1. MacDonald IC, Ragan DM, Schmidt EE, Groom AC. Kinetics of red blood cell passage
682 through interendothelial slits into venous sinuses in rat spleen, analyzed by in vivo
683 microscopy. *Microvasc Res*. 1987;33(1):118-134.
684 2. Bratosin D, Mazurier J, Tissier JP, et al. Cellular and molecular mechanisms of senescent
685 erythrocyte phagocytosis by macrophages. A review. *Biochimie*. 1998;80(2):173-195.
686 3. Mebius RE, Kraal G. Structure and function of the spleen. *Nat Rev Immunol*. 2005;5(8):606-
687 616.
688 4. Geijtenbeek TB, Groot PC, Nolte MA, et al. Marginal zone macrophages express a murine
689 homologue of DC-SIGN that captures blood-borne antigens in vivo. *Blood*.
690 2002;100(8):2908-2916.
691 5. Elomaa O, Kangas M, Sahlberg C, et al. Cloning of a novel bacteria-binding receptor
692 structurally related to scavenger receptors and expressed in a subset of macrophages. *Cell*.
693 1995;80(4):603-609.
694 6. Kraal G, Janse M. Marginal metallophilic cells of the mouse spleen identified by a
695 monoclonal antibody. *Immunology*. 1986;58(4):665-669.
696 7. Munday J, Floyd H, Crocker PR. Sialic acid binding receptors (siglecs) expressed by
697 macrophages. *J Leukoc Biol*. 1999;66(5):705-711.
698 8. Martin F, Kearney JF. Marginal-zone B cells. *Nat Rev Immunol*. 2002;2(5):323-335.
699 9. Borges da Silva H, Fonseca R, Pereira RM, Cassado Ados A, Alvarez JM, D'Imperio Lima
700 MR. Splenic macrophage subsets and their function during blood-borne infections. *Front*
701 *Immunol*. 2015;6:480.
702 10. Koppel EA, Litjens M, van den Berg VC, van Kooyk Y, Geijtenbeek TB. Interaction of
703 SIGNR1 expressed by marginal zone macrophages with marginal zone B cells is essential to
704 early IgM responses against Streptococcus pneumoniae. *Mol Immunol*. 2008;45(10):2881-
705 2887.
706 11. Bronte V, Pittet MJ. The spleen in local and systemic regulation of immunity. *Immunity*.
707 2013;39(5):806-818.
708 12. Parker KL, Schimmer BP. Steroidogenic factor 1: a key determinant of endocrine
709 development and function. *Endocr Rev*. 1997;18(3):361-377.
710 13. Morohashi K, Tsuboi-Asai H, Matsushita S, et al. Structural and functional abnormalities in
711 the spleen of an mFtz-F1 gene-disrupted mouse. *Blood*. 1999;93(5):1586-1594.

712 14. Luo X, Ikeda Y, Parker KL. A cell-specific nuclear receptor is essential for adrenal and
713 gonadal development and sexual differentiation. *Cell*. 1994;77(4):481-490.
714 15. Kalucka J, de Rooij L, Goveia J, et al. Single-cell transcriptome atlas of murine endothelial
715 cells. *Cell*. 2020;180(4):764-779 e720.
716 16. Morohashi KI, Omura T. Ad4BP/SF-1, a transcription factor essential for the transcription
717 of steroidogenic cytochrome P450 genes and for the establishment of the reproductive
718 function. *FASEB J*. 1996;10(14):1569-1577.
719 17. Pabst O, Zweigerdt R, Arnold HH. Targeted disruption of the homeobox transcription factor
720 Nkx2-3 in mice results in postnatal lethality and abnormal development of small intestine
721 and spleen. *Development*. 1999;126(10):2215-2225.
722 18. Wang CC, Biben C, Robb L, et al. Homeodomain factor Nkx2-3 controls regional expression
723 of leukocyte homing coreceptor MAdCAM-1 in specialized endothelial cells of the viscera.
724 *Dev Biol*. 2000;224(2):152-167.
725 19. Tarlinton D, Light A, Metcalf D, Harvey RP, Robb L. Architectural defects in the spleens of
726 Nkx2-3-deficient mice are intrinsic and associated with defects in both B cell maturation and
727 T cell-dependent immune responses. *J Immunol*. 2003;170(8):4002-4010.
728 20. Kellermayer Z, Labadi A, Czompoly T, Arnold HH, Balogh P. Absence of Nkx2-3
729 homeodomain transcription factor induces the formation of LYVE-1-positive endothelial
730 cysts without lymphatic commitment in the spleen. *J Histochem Cytochem*. 2011;59(7):690-
731 700.
732 21. Gabris F, Kiss G, Szirmay B, et al. Absence of Nkx2-3 induces ectopic lymphatic endothelial
733 differentiation associated with impaired extramedullary stress hematopoiesis in the spleen.
734 *Front Cell Dev Biol*. 2023;11:1170389.
735 22. Miyabayashi K, Tokunaga K, Otake H, Baba T, Shima Y, Morohashi K. Heterogeneity of
736 ovarian theca and interstitial gland cells in mice. *PLoS One*. 2015;10(6):e0128352.
737 23. Sasaki G, Ishii T, Jeyasuria P, et al. Complex role of the mitochondrial targeting signal in the
738 function of steroidogenic acute regulatory protein revealed by bacterial artificial
739 chromosome transgenesis in vivo. *Mol Endocrinol*. 2008;22(4):951-964.
740 24. Jinek M, Chylinski K, Fonfara I, Hauer M, Doudna JA, Charpentier E. A programmable
741 dual-RNA-guided DNA endonuclease in adaptive bacterial immunity. *Science*.
742 2012;337(6096):816-821.
743 25. Shima Y, Miyabayashi K, Mori T, et al. Intronic enhancer is essential for Nr5a1 expression
744 in the pituitary gonadotrope and for postnatal development of male reproductive organs in a

745 mouse model. *Int J Mol Sci*. 2022;24(1):192.
746 26. Shima Y, Miyabayashi K, Sato T, et al. Fetal Leydig cells dedifferentiate and serve as adult
747 Leydig stem cells. *Development*. 2018;145(23):dev169136.
748 27. Hao Y, Stuart T, Kowalski MH, et al. Dictionary learning for integrative, multimodal and
749 scalable single-cell analysis. *Nat Biotechnol*. 2024;42(2):293-304.
750 28. McGinnis CS, Murrow LM, Gartner ZJ. DoubletFinder: Doublet detection in single-cell
751 RNA sequencing data using artificial nearest neighbors. *Cell Syst*. 2019;8(4):329-337 e324.
752 29. Korsunsky I, Millard N, Fan J, et al. Fast, sensitive and accurate integration of single-cell
753 data with Harmony. *Nat Methods*. 2019;16(12):1289-1296.
754 30. Wu T, Hu E, Xu S, et al. clusterProfiler 4.0: A universal enrichment tool for interpreting
755 omics data. *Innovation (Camb)*. 2021;2(3):100141.
756 31. Gamliel H, Golomb HM, Avinoah E, Gurfel D, Polliack A. Topical modes in the preparation
757 of human spleen specimens for routine scanning electron microscopy studies. *Scan Electron*
758 *Microsc*. 1986;Pt 3(Pt 3):1039-1050.
759 32. Fujita T. A scanning electron microscope study of the human spleen. *Arch Histol Jpn*.
760 1974;37(3):187-216.
761 33. Zhou Y, Zhou B, Pache L, et al. Metascape provides a biologist-oriented resource for the
762 analysis of systems-level datasets. *Nat Commun*. 2019;10(1):1523.
763 34. Yahagi A, Iseki M, Yaku K, et al. Aberrant humoral immune responses and intestinal
764 homeostasis in Cd38 Bst1 double knockout mice. *Immunohorizons*. 2025;9(8):vlaf029.
765 35. Han S, Baba T, Yanai S, et al. GC-MS-based metabolic signatures reveal comparative
766 steroidogenic pathways between fetal and adult mouse testes. *Andrology*. 2021;9(1):400-406.
767 36. Noh J, Lee C, Kim JH, Myung SW, Choi MH. LC-MS based simultaneous profiling of
768 adrenal hormones of steroids, catecholamines, and metanephrines. *J Lipid Res*.
769 2023;64(11):100453.
770 37. Kraal G, Schornagel K, Streeter PR, Holzmann B, Butcher EC. Expression of the mucosal
771 vascular addressin, MAdCAM-1, on sinus-lining cells in the spleen. *Am J Pathol*.
772 1995;147(3):763-771.
773 38. Libby JR, Royce H, Walker SR, Li L. The role of extracellular matrix in angiogenesis:
774 Beyond adhesion and structure. *Biomater Biosyst*. 2024;15:100097.
775 39. Goveia J, Rohlenova K, Taverna F, et al. An integrated gene expression landscape profiling
776 approach to identify lung tumor endothelial cell heterogeneity and angiogenic candidates.
777 *Cancer Cell*. 2020;37(1):21-36 e13.

40. Geldhof V, de Rooij L, Sokol L, et al. Single cell atlas identifies lipid-processing and immunomodulatory endothelial cells in healthy and malignant breast. *Nat Commun*. 2022;13(1):5511.
41. Kang B, Camps J, Fan B, et al. Parallel single-cell and bulk transcriptome analyses reveal key features of the gastric tumor microenvironment. *Genome Biol*. 2022;23(1):265.
42. Zeng Q, Mousa M, Nadukkandy AS, et al. Understanding tumour endothelial cell heterogeneity and function from single-cell omics. *Nat Rev Cancer*. 2023;23(8):544-564.
43. Francavilla C, Maddaluno L, Cavallaro U. The functional role of cell adhesion molecules in tumor angiogenesis. *Semin Cancer Biol*. 2009;19(5):298-309.
44. Shima Y, Zubair M, Ishihara S, et al. Ventromedial hypothalamic nucleus-specific enhancer of Ad4BP/SF-1 gene. *Mol Endocrinol*. 2005;19(11):2812-2823.
45. Zubair M, Ishihara S, Oka S, Okumura K, Morohashi K. Two-step regulation of Ad4BP/SF-1 gene transcription during fetal adrenal development: initiation by a Hox-Pbx1-Prep1 complex and maintenance via autoregulation by Ad4BP/SF-1. *Mol Cell Biol*. 2006;26(11):4111-4121.
46. Shima Y, Zubair M, Komatsu T, et al. Pituitary homeobox 2 regulates adrenal4 binding protein/steroidogenic factor-1 gene transcription in the pituitary gonadotrope through interaction with the intronic enhancer. *Mol Endocrinol*. 2008;22(7):1633-1646.
47. Shima Y, Miyabayashi K, Baba T, et al. Identification of an enhancer in the Ad4BP/SF-1 gene specific for fetal Leydig cells. *Endocrinology*. 2012;153(1):417-425.
48. Menees KB, Earls RH, Chung J, et al. Sex- and age-dependent alterations of splenic immune cell profile and NK cell phenotypes and function in C57BL/6J mice. *Immun Ageing*. 2021;18(1):3.
49. Czompoly T, Labadi A, Kellermayer Z, Olasz K, Arnold HH, Balogh P. Transcription factor Nkx2-3 controls the vascular identity and lymphocyte homing in the spleen. *J Immunol*. 2011;186(12):6981-6989.
50. Lewis SM, Williams A, Eisenbarth SC. Structure and function of the immune system in the spleen. *Sci Immunol*. 2019;4(33):eaau6085.
51. Kraal G, Mebius R. New insights into the cell biology of the marginal zone of the spleen. *Int Rev Cytol*. 2006;250:175-215.
52. Hassanpour M, Salybekov AA, Kobayashi S, Asahara T. CD34 positive cells as endothelial progenitor cells in biology and medicine. *Front Cell Dev Biol*. 2023;11:1128134.
53. Dunn SE, Perry WA, Klein SL. Mechanisms and consequences of sex differences in immune

811 responses. *Nat Rev Nephrol*. 2024;20(1):37-55.
812 54. Katoh-Fukui Y, Owaki A, Toyama Y, et al. Mouse Polycomb M33 is required for splenic
813 vascular and adrenal gland formation through regulating Ad4BP/SF1 expression. *Blood*.
814 2005;106(5):1612-1620.
815 55. Fatchiyah, Zubair M, Shima Y, et al. Differential gene dosage effects of Ad4BP/SF-1 on
816 target tissue development. *Biochem Biophys Res Commun*. 2006;341(4):1036-1045.
817 56. Kim S, Wysocka J. Deciphering the multi-scale, quantitative cis-regulatory code. *Mol Cell*.
818 2023;83(3):373-392.
819 57. Achermann JC, Ito M, Ito M, Hindmarsh PC, Jameson JL. A mutation in the gene encoding
820 steroidogenic factor-1 causes XY sex reversal and adrenal failure in humans. *Nat Genet*.
821 1999;22(2):125-126.
822 58. Camats N, Pandey AV, Fernandez-Cancio M, et al. Ten novel mutations in the NR5A1 gene
823 cause disordered sex development in 46,XY and ovarian insufficiency in 46,XX individuals.
824 *J Clin Endocrinol Metab*. 2012;97(7):E1294-1306.
825

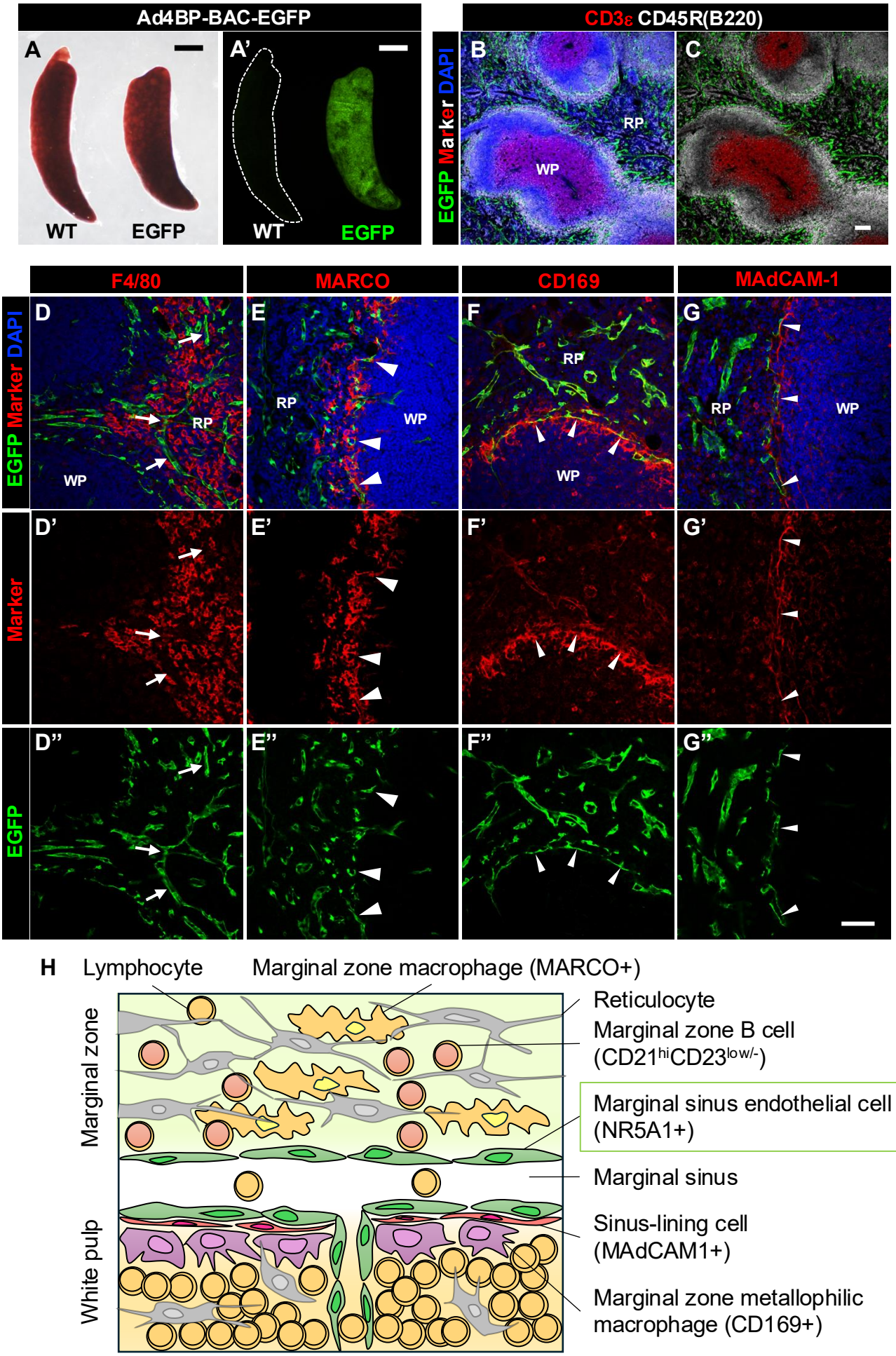

Miyabayashi, et al., Figure 1

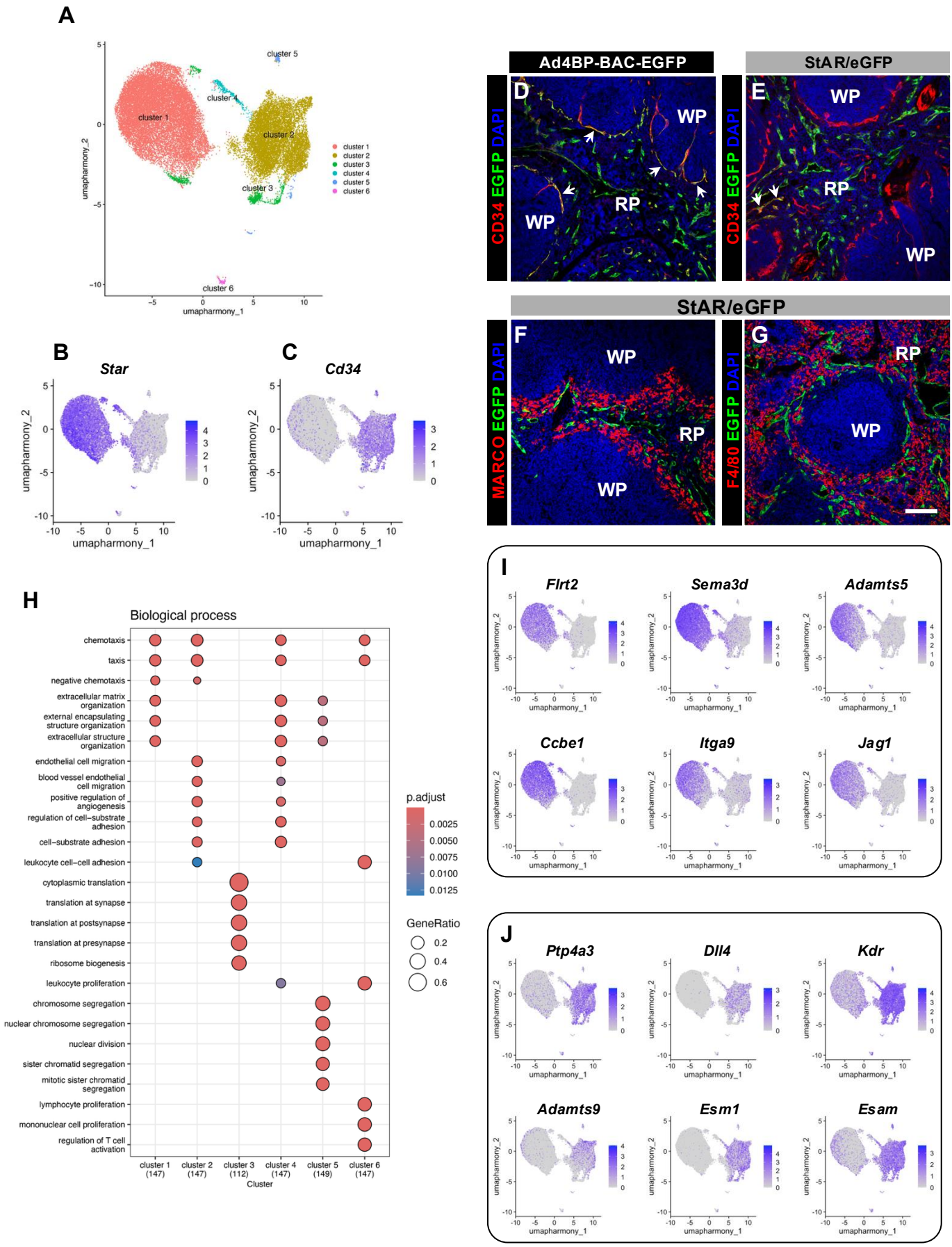

Miyabayashi, et al., Figure 2

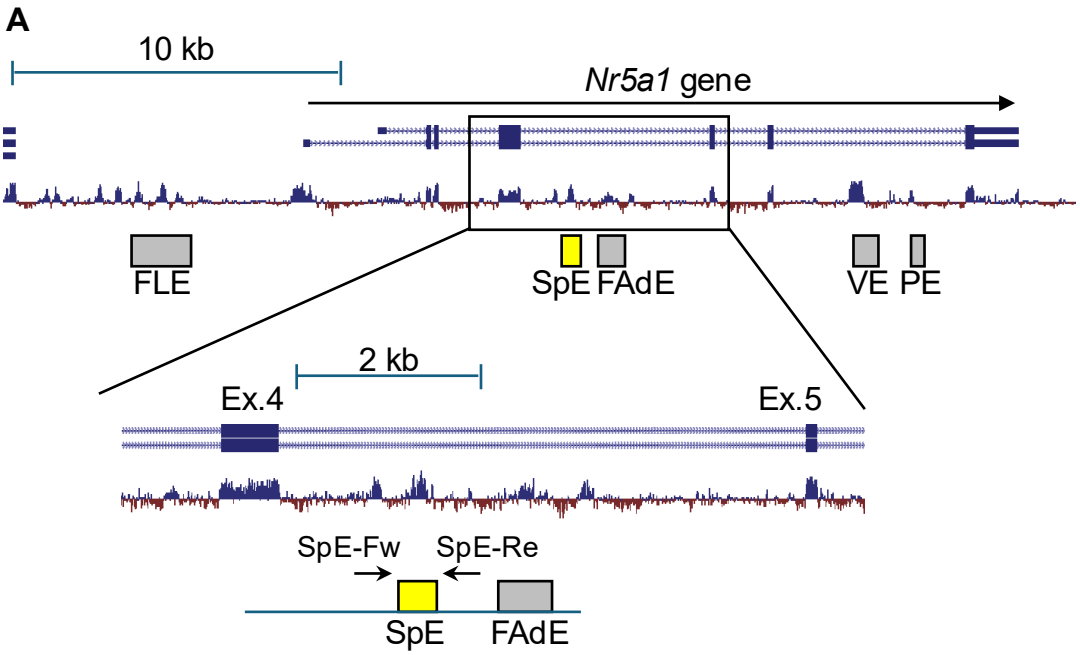

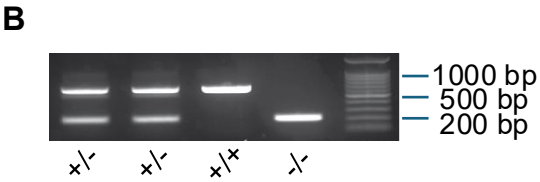

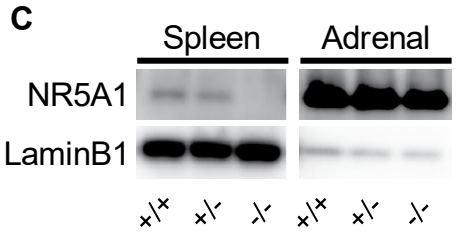

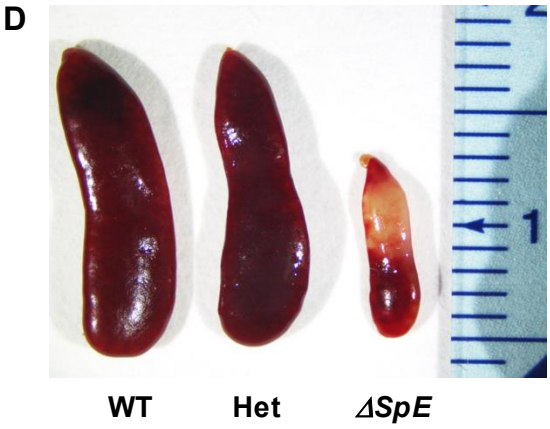

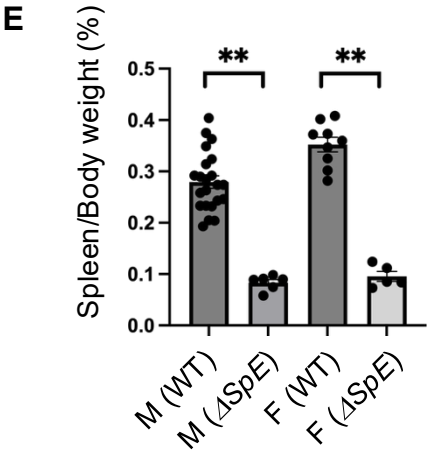

Miyabayashi, et al., Figure 3

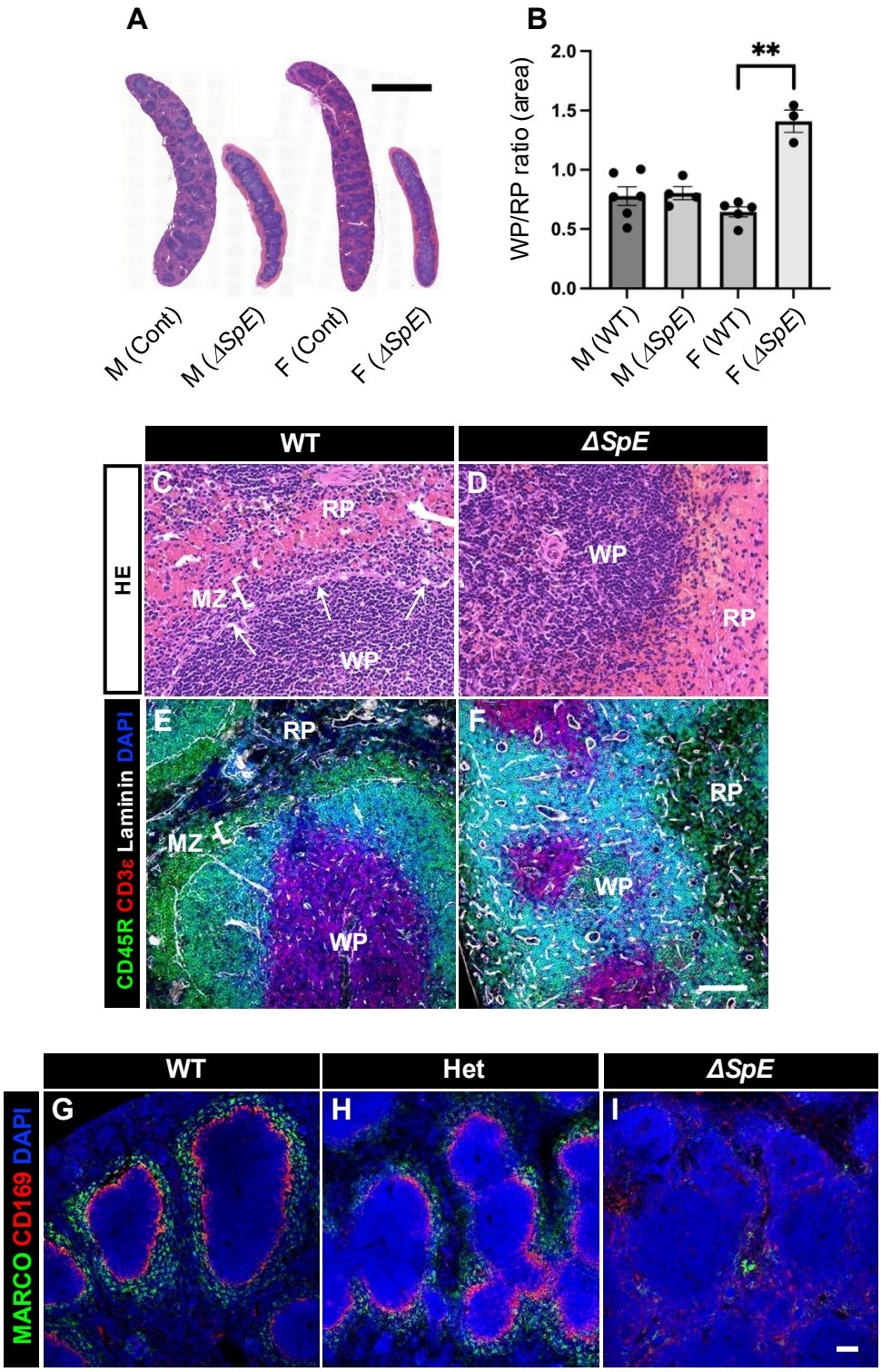

Miyabayashi, et al., Figure 4

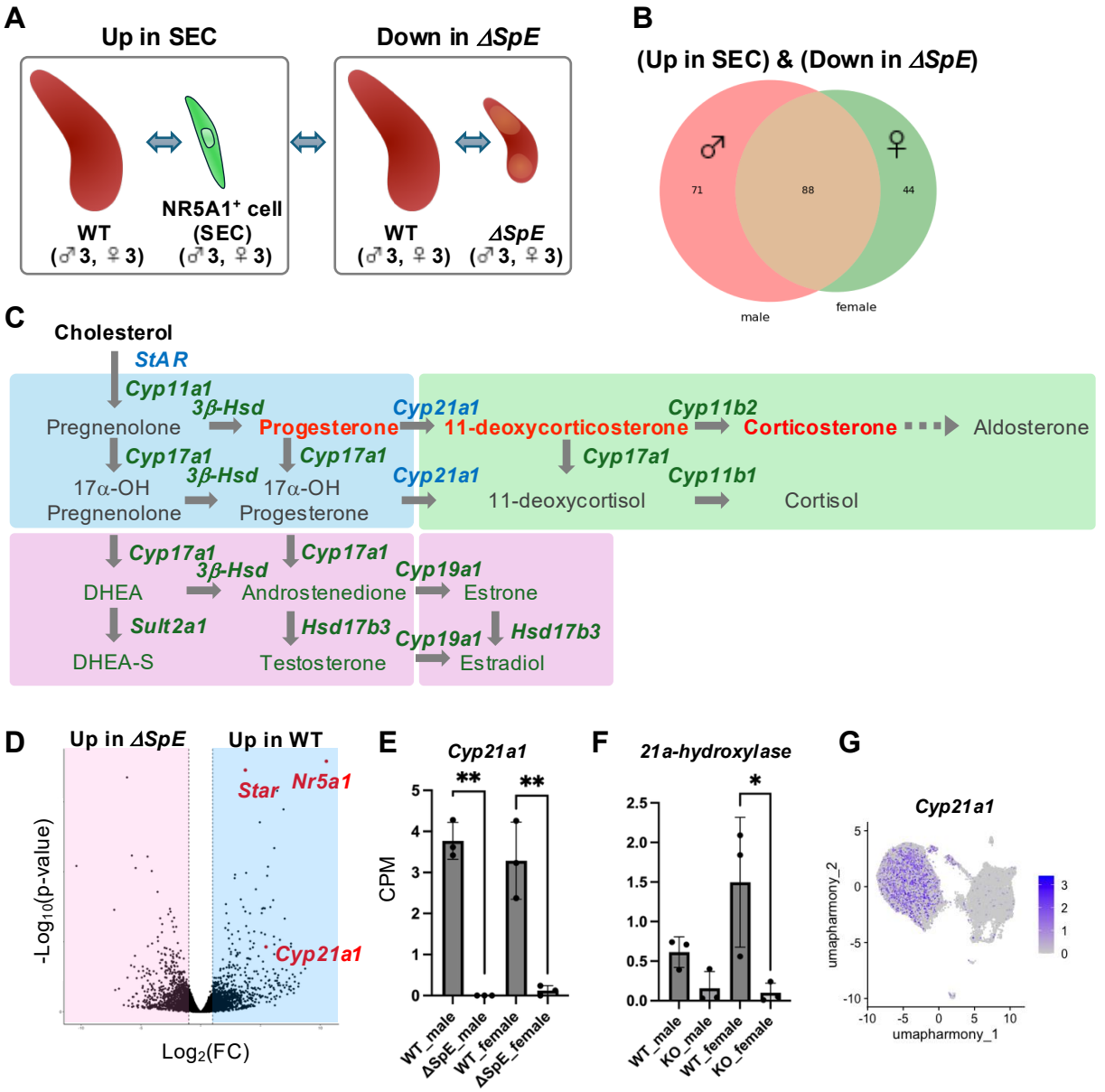

Miyabayashi, et al., Figure 5

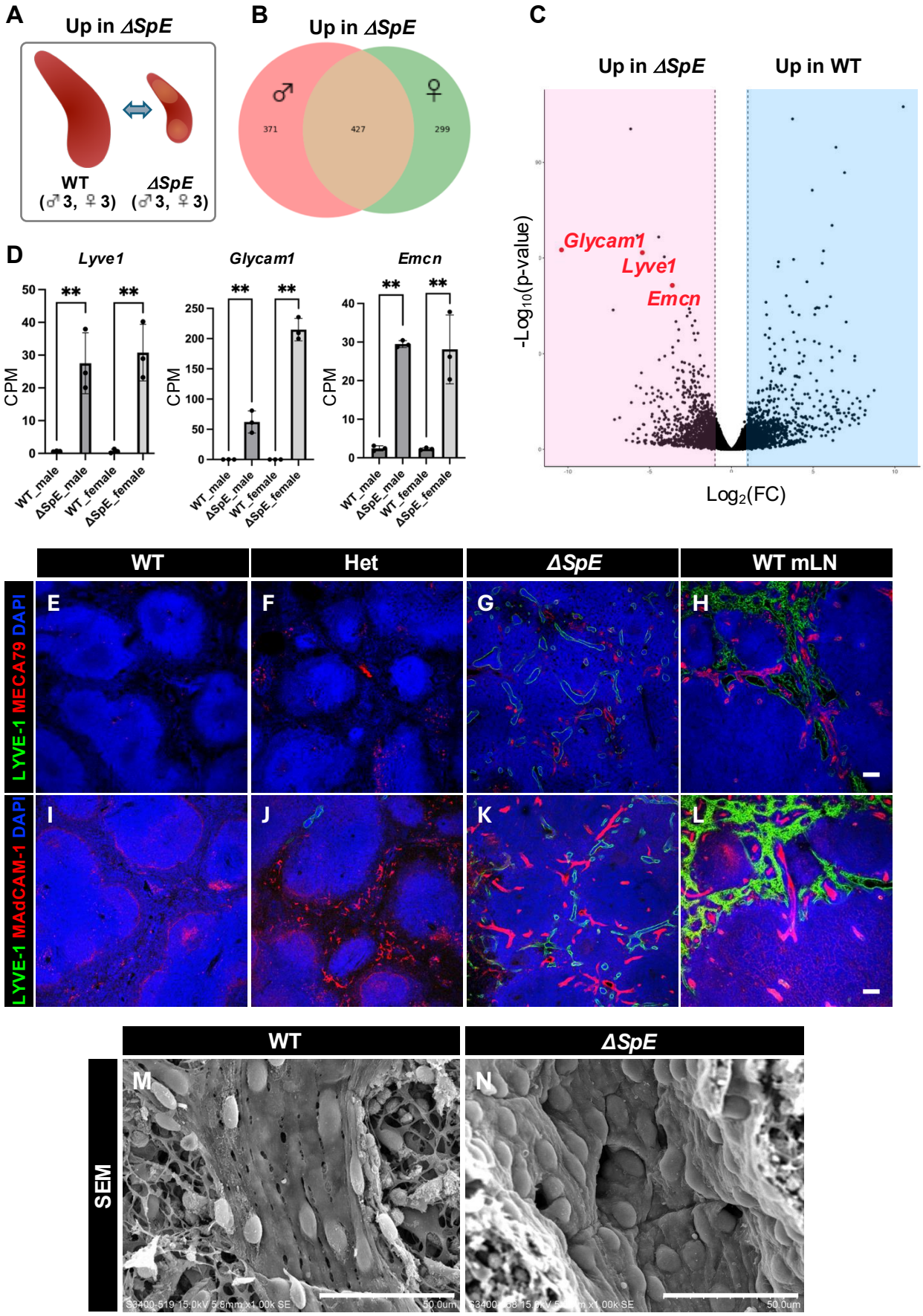

Miyabayashi, et al., Figure 6

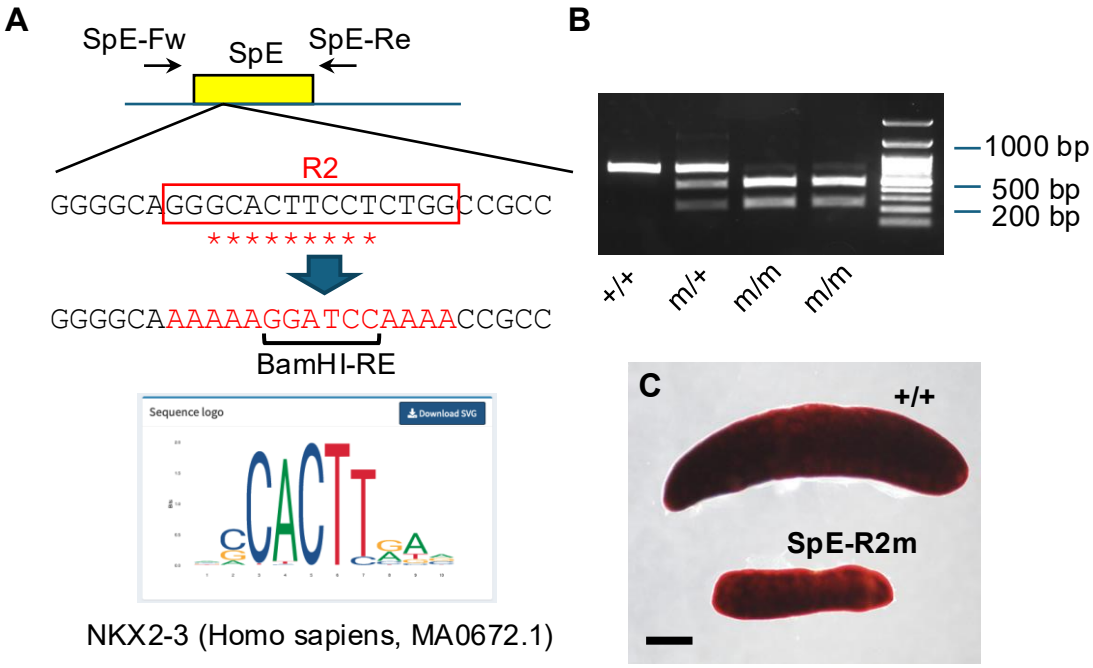

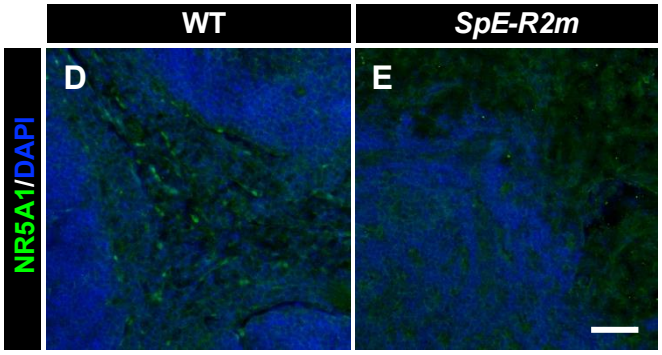

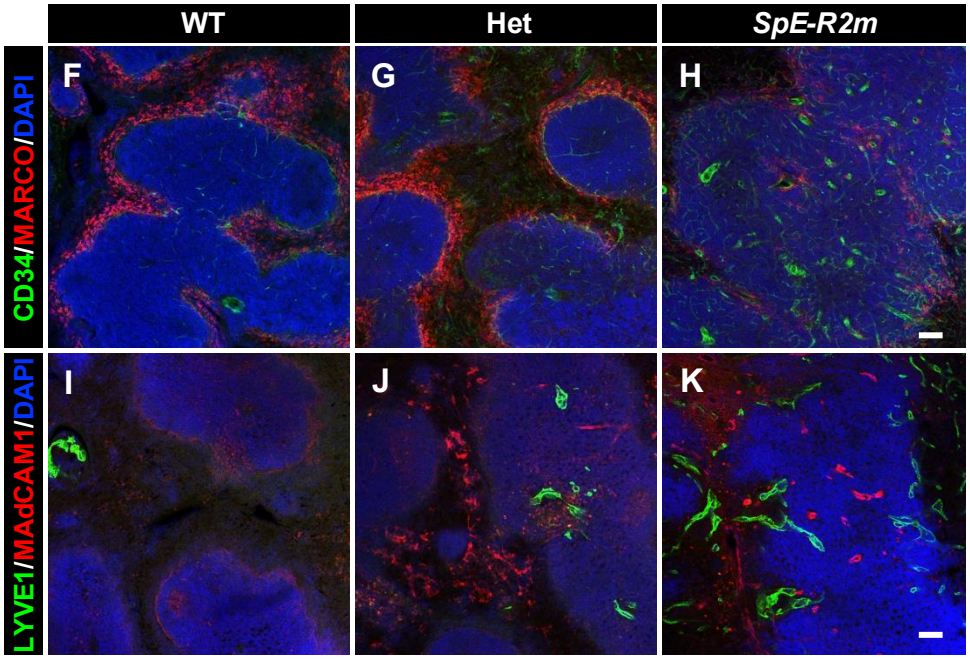

Miyabayashi, et al., Figure 7